


# *In silico* discovery of SARS-CoV-2 main protease inhibitors from the carboline and quinoline database

Eldar Muhtar<sup>1</sup> , Mengyang Wang<sup>1</sup>  & Haimei Zhu<sup>\*,1</sup> 

<sup>1</sup>Beijing Area Major Laboratory of Peptide & Small Molecular Drugs, Engineering Research Center of Endogenous Prophylactic of Ministry of Education of China, Beijing Laboratory of Biomedical Materials, College of Pharmaceutical Sciences of Capital Medical University, Beijing, 100069, China

\*Author for correspondence: [hmzhu@ccmu.edu.cn](mailto:hmzhu@ccmu.edu.cn)

**Aim:** SARS-CoV-2 caused more than 3.8 million deaths according to the WHO. In this urgent circumstance, we aimed at screening out potential inhibitors targeting the main protease of SARS-CoV-2. **Materials & methods:** An in-house carboline and quinoline database including carboline, quinoline and their derivatives was established. A virtual screening in carboline and quinoline database, 50 ns molecular dynamics simulations and molecular mechanics Poisson–Boltzmann surface area calculations were carried out. **Results:** The top 12 molecules were screened out preliminarily. The molecular mechanics Poisson–Boltzmann surface area ranking showed that p59\_7m, p12\_7e, p59\_7k stood out with the lowest binding energies of -24.20, -17.98, -17.67 kcal/mol, respectively. **Conclusion:** The study provides powerful *in silico* results that indicate the selected molecules are valuable for further evaluation as SARS-CoV-2 main protease inhibitors.

First draft submitted: 26 April 2021; Accepted for publication: 5 July 2021; Published online: 20 July 2021

**Keywords:** carboline • dPCA • main protease • MD simulation • MM-PBSA • SARS-CoV-2 • virtual screening

SARS-CoV-2 has spread all over the world, led to SARS and caused more than 179 million infections and 3.8 million deaths according to the WHO [1]. SARS-CoV-2 manifests higher transmissibility and lower mortality compared with SARS-CoV. SARS-CoV-2 shows efficient intrafamilial spread [2]. Although, several vaccines have been approved by the WHO such as BBIBP-CoV and CoronaVac [3], the pain and fever occur after treatment of some vaccines. The protective efficacy of the vaccines still need to be improved. Vaccines can help to prevent infection and severe symptoms caused by SARS-CoV-2. However, for patients who have been infected with the virus, drugs are still in need. Remdesivir is the first drug approved by the US FDA for the treatment of SARS-CoV-2 [4]. Remdesivir targets RNA polymerase to inhibit viral replication. However, main protease ( $M^{pro}$ ) is also one of the most important enzymes in the life cycle of virus.  $M^{pro}$  of SARS-CoV-2 is a crucial enzyme of coronaviruses and has a pivotal role in mediating the viral maturation [5]. Besides,  $M^{pro}$  is most abundant in the viral surface and is believed to be the crucial organizer in the coronavirus assembly [6], making it an arresting drug target for SARS-CoV-2. The protein crystal (Protein Data Bank [PDB] code: 6LU7) contains ligand N3 which help us to define the active site pocket of  $M^{pro}$  of SARS-CoV-2 [7]. Docking is useful in virtual screening of small molecule databases and predicting the structures and functions of biomolecular complexes. Molecular dynamics (MD) simulations can give a dynamic image that obtained from the molecular docking [8]. Moreover, the molecular mechanics Poisson–Boltzmann surface area (MM-PBSA) method provides a more accurate calculation of the binding energy. In previous studies, molecules in public databases, repurposed approved drugs or molecules in natural products were obtained for *in silico* screening targeting  $M^{pro}$  [9–14]. We established an in-house database, carboline and quinoline database (CQDB) that included both carboline and quinoline molecules in this study. Since isoquinoline, quinoline,  $\beta$ -carboline and their derivatives show the powerful antiviral bioactivity [15,16]. Based on the small molecule database, we attend to use computational approaches mentioned above to find potential molecules for the treatment of SARS-CoV-2 (Figure 1).

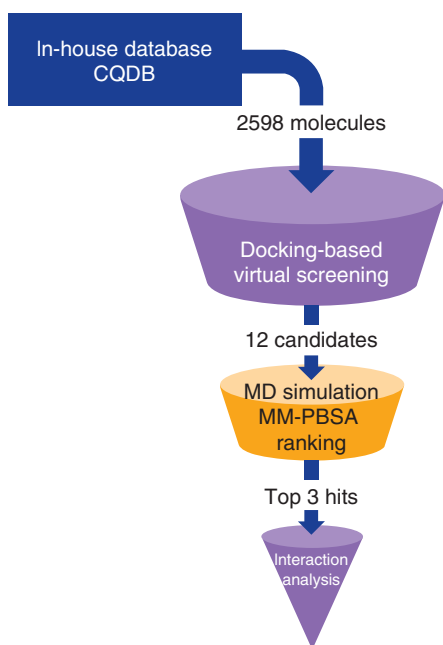


**Figure 1. Workflow for the discovery of potential inhibitor against main protease *in silico*.**

CQDB: Carboline and quinoline database; MD: Molecular dynamics; MM-PBSA: Molecular mechanics Poisson–Boltzmann surface area.

## Materials & methods

### Dataset

For this study, we established a small molecule database named "CQDB". CQDB includes 2598 carboline and quinoline derivatives without duplicated molecules. 1117 molecules were synthesized and patented in our previous work. Another 1481 molecules were obtained from the publications of other pharmaceutical researches. 2D structures of these molecules were sketched in ChemBioDraw and converted to 3D structures with Open Babel v3.1.0 as ligands [17]. Afterward, optimizations were done in 250 steps of a steepest-descent geometry optimization with the MMFF94 forcefield in Open Babel.

### Protein & ligand setup

The crystal structure of SARS-CoV-2 M<sup>Pro</sup> (PDB code: 6LU7) was obtained from the PDB with a resolution of 2.16 angstrom. The protease consisted of one chain with 306 amino acids. 6LU7 was prepared at a pH level of 7.4 for protonation using the 'prepare protein' protocol in BIOVIA Discovery Studio 2016 (Dassault Systèmes, Vélizy-Villacoublay, France). The protonation state of crucial residuals such as HIS 41, HIS 164 and GLU 166 in binding-site was checked carefully again. The solvent was stripped off. Ligands were obtained from the CQDB database.

### Docking-based virtual screening

Docking-based virtual screening, which is one of the most promising methods *in silico* for the drug-like molecule discovery, is useful to predict the best interaction state between a ligand and a protein. AutoDock Vina (Scripps Research, CA, USA) was chosen to perform the virtual screening. Since AutoDock Vina provides the maximum accuracy and the minimum computer time, which refers to the empirical and knowledge-based scoring functions [18]. Ligands were assigned with the gasteiger charges. The grid box size in three dimensions was  $40 \times 40 \times 40$  Å with a center coordinate of -7.857, 11.856 and 67.687, which was the center of the ligand N3 in the crystal structure. The exhaustiveness of the global search was increased to 12. Based on the binding affinity ranking, the top 12 molecules that satisfied a threshold ( $\Delta G \leq -9.8$  kcal/mol) were screened out for more detailed analysis.

### Strategy of docking & selection of promising configuration

In the docking analysis, a theoretical method to identify the appropriate configuration of ligand in enzyme active-site is very important [19,20]. To evaluate the docking and selection strategy, N3 was fetched out from the crystal structure and redocked into M<sup>Pro</sup> as a reference. Covalent docking was performed using AutoDock 4.2.6 [21]. The grid box dimensions were  $40 \times 40 \times 40$  Å. The grid spacing was set as 0.375 Å. Lamarckian genetic algorithm was

utilized to find the appropriate configurations of ligands. The global optimization was performed with parameters of 300 randomly positioned individuals. The maximum number of energy evaluations was enhanced to  $2.5 \times 10^7$ , and the maximum number of generations in lamarkian genetic algorithm was enhanced to  $2.7 \times 10^5$ . The Solis and Wets local search was executed with a maximum number of 3000. During docking experiments 200 runs were carried out. The resulted 200 conformations of each were ranked by the lowest binding energy and clustered with an all-atom root mean square deviation tolerance of 2.0 Å. The lowest binding energy, the population of the configuration in the cluster analysis and the proper binding mode were considered comprehensively for selecting the promising configuration of N3. Subsequently, the top 12 molecules were redocked toward the M<sup>Pro</sup> in AutoDock 4.2.6 to select the promising configurations using the same selection strategy. The selected promising configurations of the 12 molecules were submitted as the start configurations for the MD simulations.

### MD simulation analysis

MD simulation is a decision-making procedure for the evaluation of complex stability [22]. It is useful in the investigation of the dynamic behavior at an atomic level of biological systems, which is hard to process in the laboratory [23]. In the present study, the most promising configurations of the 12 M<sup>Pro</sup>-ligand complexes were chosen as the starting point for MD simulations. MD simulations for 12 M<sup>Pro</sup>-ligand complexes and an apo form of the M<sup>Pro</sup> were performed on a 50 ns time scale. The CHARMM General Force Field web-based tool (<https://cgenff.umaryland.edu/>) was used to generate ligand parameter files. Charge of ligands was assigned by the extended bond-charge increment scheme [24]. Gromacs 2020.1 was utilized to perform the simulation with the CHARMM36 all-atom force field [25,26]. All of the 13 systems were solvated with an extended simple point charge model (SPC/E) and neutralized via adding Na<sup>+</sup> ions [27]. In the following process, the energy of the system was minimized by the steepest descent algorithm at a threshold of 1000 kJ.mol<sup>-1</sup>.nm<sup>-1</sup>. Then two-part equilibration, conserved moles, volume and temperature (NVT) and conserved moles, pressure and temperature (NPT) ensembles were done for 0.5 ns. Long-range electrostatics was calculated by the particle Mesh Ewald method [28]. About 50 ns MD simulations were performed at a time step of 2 fs. Then root mean square deviation (RMSD), root mean square fluctuation (RMSF), radius of gyration (Rg) and the number of hydrogen bonds were calculated to analyze the MD trajectories in GROMACS utilities.

### MM-PBSA combined with MD

MM-PBSA is used in study of biomolecular interactions and the computational drug design. MM-PBSA binding energy of chosen molecules was calculated via g\_mmpbsa [29]. This tool calculates the enthalpic components of the MM-PBSA interaction using GROMACS and the APBS packages. The total binding free energy is calculated as follows:  $\Delta G_{binding} = G_{complex} - (G_{protein} + G_{ligand})$

### Dihedral angle principal component analysis

The principal component analysis (PCA) method was used to calculate eigenvectors and eigenvalues and their projection along with the first two principal components during MD simulation. The dihedral angle principal component analysis (dPCA), which is based on the Gromacs protocol, uses backbone dihedral angles to analyze while PCA uses Cartesian coordinates [25]. dPCA can readily be characterized by the corresponding conformational changes of peptides in a protein [30]. dPCA was calculated from the MD backbone trajectories. Via diagonalizing the matrix, a bunch of eigenvectors and eigenvalues were generated and plotted in the 2D projection to evaluate the motion of trajectory.

## Results

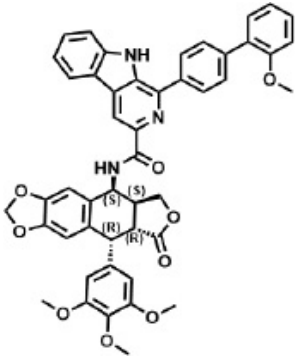
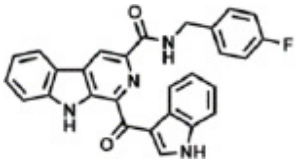
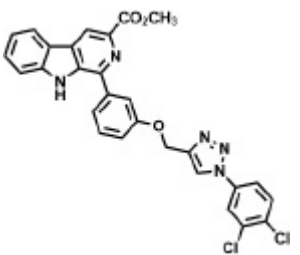
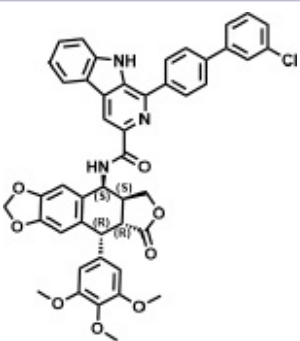
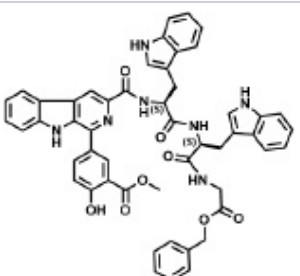
### Virtual screening

To evaluate the potential of molecules in our database to become inhibitors of M<sup>Pro</sup>, AutoDock Vina was used to screen in the database and rank molecules according to their binding affinities. The name, structure and molecular weight of the top 12 molecules are listed in Table 1.

### Selection of proper configurations of referenced inhibitor

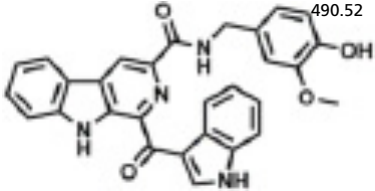
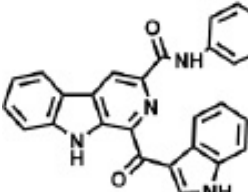
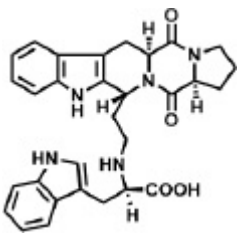
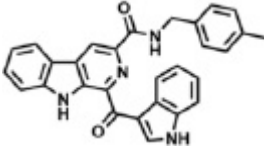
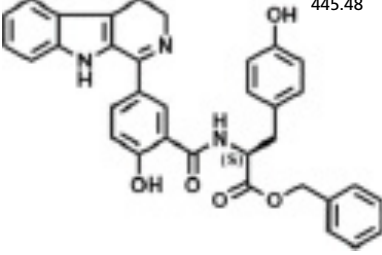
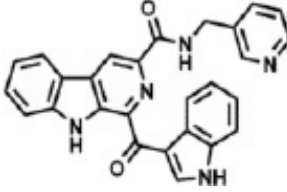
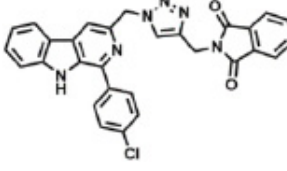
The proper docked configuration of N3 was selected and shown in Figure 2. The selected configuration of N3 is well overlapped with N3 in the crystal structure. The binding free energy of the selected configuration of N3 to the M<sup>Pro</sup> is -15.40 kcal/mol in AutoDock 4.2.6. Compared with the crystal N3, the selected configuration of N3

Table 1. The name, structure, molecular weight and binding free energies of the top 12 molecules virtually screened from in-house carboline and quinoline database.

Rank	Name	Structure	Molecular weight	$\Delta G$ from AutoDock (kcal/mol)	$\Delta G$ from MM-PBSA (kcal/mol)
1	p59.7m		789.84	-8.39	-24.20
2	p63.9h		462.48	-8.60	-17.98
3	p12.7e		544.39	-9.10	-17.67
4	p59.7k		794.26	-8.70	-17.51
5	22.7b		881.95	-5.55	-16.44

Binding free energies calculated with both AutoDock and MM-PBSA. The top 12 molecules ranked by MM-PBSA binding energy. MM-PBSA: Molecular mechanics Poisson–Boltzmann surface area.

**Table 1.** The name, structure, molecular weight and binding free energies of the top 12 molecules virtually screened from in-house carboline and quinoline database. (cont.).

Rank	Name	Structure	Molecular weight	$\Delta G$ from AutoDock (kcal/mol)	$\Delta G$ from MM-PBSA (kcal/mol)
6	p63.9l		490.52	-8.22	-16.07
7	p63.9m		448.46	-8.28	-14.55
8	506.4Rd		525.61	-7.10	-13.48
9	p63.9i		458.52	-8.92	-12.94
10	p63.9j		445.48	-8.00	-12.24
11	310.5g		559.62	-7.82	-11.30
12	p80.7r		518.96	-9.34	-7.90

Binding free energies calculated with both AutoDock and MM-PBSA. The top 12 molecules ranked by MM-PBSA binding energy. MM-PBSA: Molecular mechanics Poisson–Boltzmann surface area.

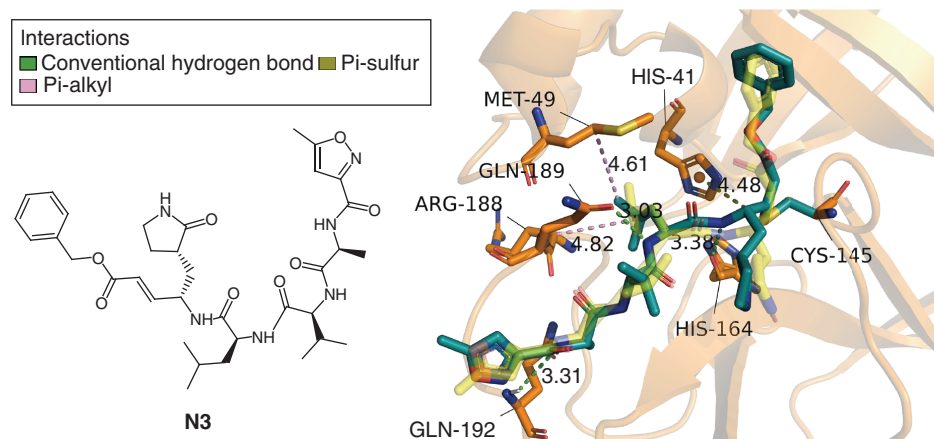


**Figure 2.** Molecular interactions between main protease (orange ribbon) and docked main protease inhibitor N3 from crystal structure 6LU7 (deep teal stick). Crystal structure of M<sup>Pro</sup> inhibitor N3 shown as yellow transparent stick model.

**Table 2.** Contributions in molecular mechanics Poisson–Boltzmann surface area binding energies of the top four molecules.

Name	$\Delta E_{\text{ele}}$	$\Delta E_{\text{vdw}}$	$\Delta G_{\text{np}}$	$\Delta G_{\text{p}}$	$\Delta G_{\text{bind}}$
p59_7m	-13.29	-51.16	-5.83	46.07	-24.20
p63_9h	-4.21	-34.70	-3.69	24.62	-17.98
p12_7e	-7.36	-45.31	-4.68	39.68	-17.67
p59_7k	-14.93	-51.48	-6.05	54.96	-17.51

The unit of all parameters is kcal/mol.

$\Delta E_{\text{ele}}$ : Electrostatic energy;  $\Delta E_{\text{vdw}}$ : Van der Waal energy;  $\Delta G_{\text{np}}$ : None polar solvation energy (solvent-accessible surface area energy);  $\Delta G_{\text{p}}$ : Polar solvation energy;  $\Delta G_{\text{bind}}$ : Binding energy.

forms similar molecular interactions with the M<sup>Pro</sup>, including conventional hydrogen bonds with GLY 143, HIS 164, GLN 189 and GLN 192, hydrophobic interactions such as Pi-Sulfur, Pi-Alkyl with MET 49 and HIS 41 and ARG 188. The result suggests that the selection strategy of proper configuration of the ligand is appropriate.

Using the same docking and selection strategy, the top 12 molecules were redocked with AutoDock 4.2.6. The most promising configurations of the 12 molecules are selected and the lowest binding energies calculated by AutoDock 4.2.6 are listed in Table 1.

### Reranking with MM-PBSA binding energy

The top 12 molecules were reranked according to the MM-PBSA binding energies shown in Table 1. The top four molecules are p59\_7m, p63\_9h, p12\_7e and p59\_7k. Figures 3A–D shows the fluctuation of MM-PBSA binding energies of the top four molecules during 50 ns MD simulations. The MM-PBSA binding energy of the top four molecules fluctuated stably during 50 ns. Table 2 shows contributions in MM-PBSA binding energy of the top four molecules.

### Binding stability evaluations during MD simulation

To evaluate the binding stability of the top 12 molecules at the binding site of M<sup>Pro</sup>, the protein backbone RMSD, RMSF, the Rg and the number of hydrogen bonds, the protein dihedral principal component (dPCA) and the ligand binding mode during 50 ns MD simulations were carefully inspected. It was found that p63\_9h exhibited unstable binding mode at the active site of the M<sup>Pro</sup>. Thus, p59\_7m, p12\_7e and p59\_7k were suggested as the top three molecules with the potential of inhibiting M<sup>Pro</sup>. The average protein backbone RMSD of apo form is 0.26 nm while holo forms with p59\_7m, p12\_7e, p59\_7k are 0.18, 0.20, 0.19 nm, respectively (Figure 4A). This result suggests the reduction of overall protein flexibility upon binding of the three selected molecules. The protein backbone RMSF shown in Figure 4B represents lower fluctuations of protein residues during MD simulation upon binding p59\_7m and p59\_7k than binding p12\_7e. The Rg shown in Figure 4C exhibits more compact protein–ligand complex during MD simulation upon binding p59\_7m and p12\_7e than binding p59\_7k. The number of

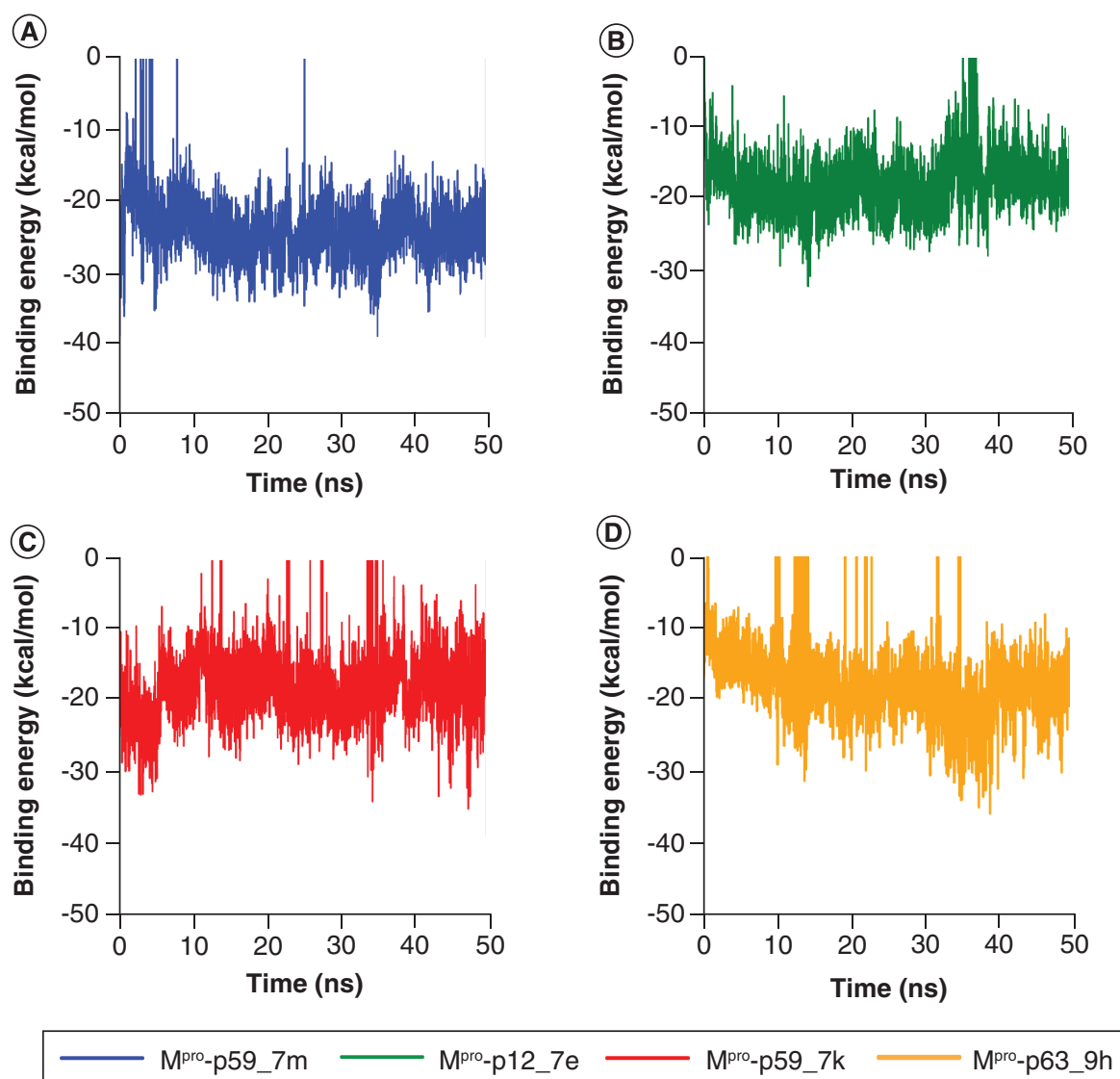


**Figure 3.** The molecular mechanics Poisson–Boltzmann surface area binding energies over 50 ns simulations of the top four ranked molecules.

M<sup>pro</sup>: Main protease.

hydrogen bonds reflects one of the crucial interactions between the protein and the corresponding ligand. As seen in Figure 4D, average number of hydrogen bonds upon binding of p59\_7m, p12\_7e, p59\_7k are 2.0, 1.2 and 1.8, respectively. This suggests p59\_7m forms stronger hydrogen bond interactions than p59\_7k and p12\_7e.

#### Dihedral principal component analysis

The dihedral principal component analysis (dPCA) method was employed to reveal the dynamical behavior in the space of SARS-CoV-2 M<sup>pro</sup> when combined with the top three molecules. The first two principal components were selected to analyze the projection of apo form phase space and holo form phase spaces with top three molecules during the 50 ns MD simulations. Figure 5 clearly shows that apo protein and the M<sup>pro</sup>-p59\_7k complex covered a larger region of phase space while the M<sup>pro</sup>-p59\_7m complex and M<sup>pro</sup>-p12\_7e complex covered smaller ones. The result suggests that binding of p59\_7m and p12\_7e in the active site limits large dynamic behaviors of SARS CoV-2 M<sup>pro</sup>, which is in accordance with the Rg results.

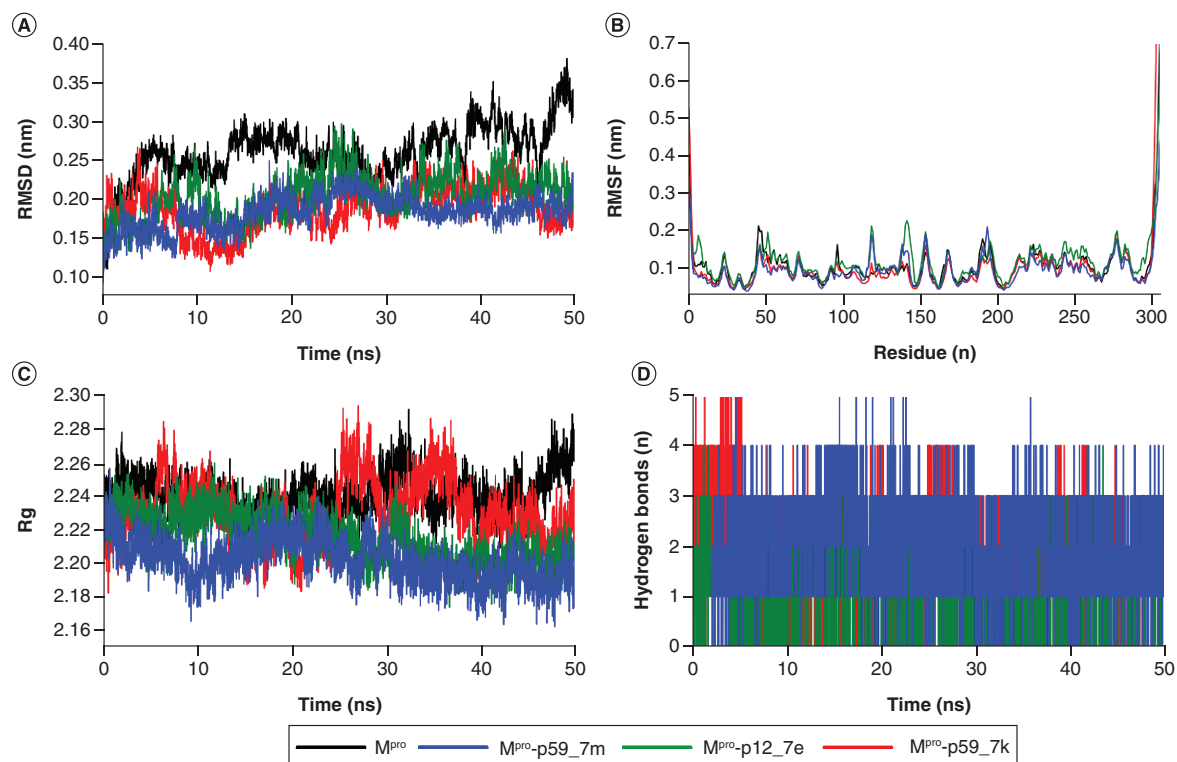


**Figure 4.** The molecular dynamics simulation analysis of apo SARS-CoV-2 main protease and three main protease–ligand complexes. (A) Root mean square deviation values of the M<sup>pro</sup> backbone over time. (B) Root mean square fluctuation values of the M<sup>pro</sup> backbone during 50 ns simulations. (C) Radius of gyration of the main protease over time. (D) Hydrogen bond number between main protease and ligands over time. M<sup>pro</sup>: Main protease; Rg: Radius of gyration; RMSD: Root mean square deviation; RMSF: Root mean square fluctuation.

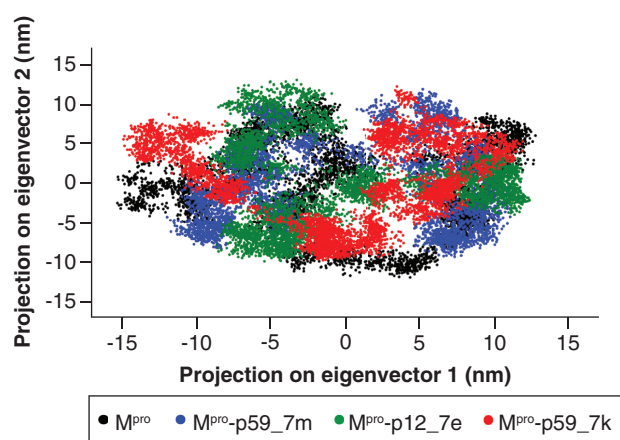


**Figure 5.** 2D projection of motion trajectory of apo SARS-CoV-2 main protease and three main protease–ligand complexes over the first two principal components. M<sup>pro</sup>: Main protease.

### Protein–ligand interaction analysis

The 3D interactions of the top three molecules with M<sup>pro</sup> in the last snapshot from MD simulation are shown in Figures 6A–C. Figure 6A reveals p59\_7m forms four conventional hydrogen bonds with THR 26, HIS 41, CYS 145, ARG 188 in range: 3.17–3.49 Å. While p12\_7e (Figure 6B) and p59\_7k (Figure 6C) forms three and two conventional hydrogen bonds with M<sup>pro</sup>, respectively. Besides, p59\_7m forms hydrophobic interactions with MET 49 and ASN 142.



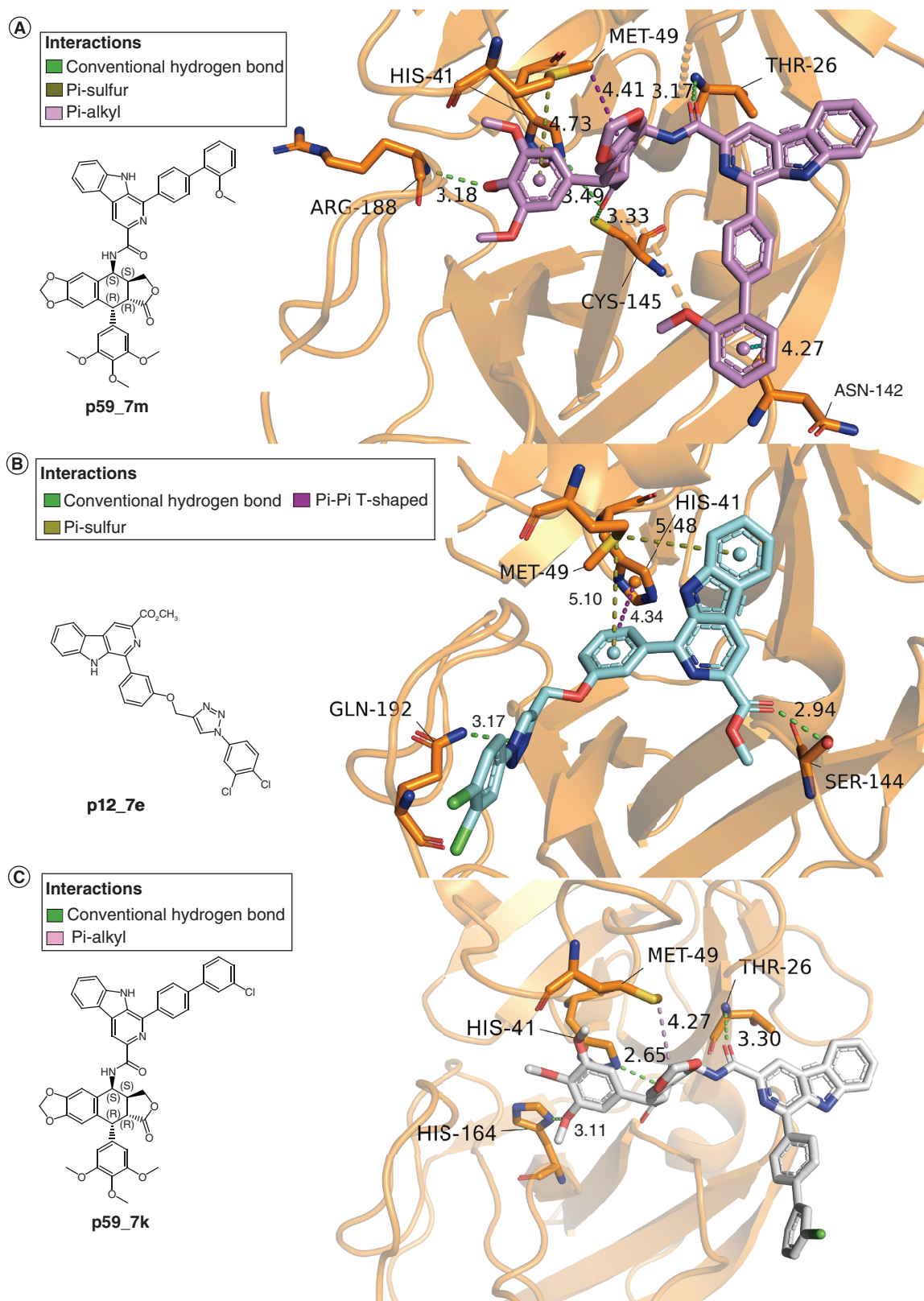


**Figure 6. Molecular interactions between main protease and the top three molecules in the last snapshots of molecular dynamics simulations. (A) p59\_7m in the active site of main protease (M<sup>PRO</sup>). (B) p12\_7e in the active site of M<sup>PRO</sup>. (C) p59\_7k in the active site of M<sup>PRO</sup>.**

## Discussion

SARS-CoV-2 invades human respiratory system, spreads rapidly and causes a severe health crisis all over the world. Vaccines can help to prevent infection and severe symptoms caused by SARS-CoV-2. However, drugs treating SARS-CoV-2 infection are still in urgent need. The RNA polymerase inhibitor, remdesivir, is the only drug approved by FDA up to now. Nowadays, The M<sup>Pro</sup> of SARS-CoV-2 has become one of the most promising targets for new drugs. The M<sup>Pro</sup> inhibitor PF-07321332 from Pfizer has entered a Phase I clinical study [31]. Carboline and quinoline molecules were reported to possess powerful antiviral bioactivities. An in-house database CQDB containing 2598 carboline and quinoline molecules was established for the discovery of M<sup>Pro</sup> inhibitors. Docking-based virtual screening and following MD simulations revealed three potential M<sup>Pro</sup> inhibitors p59\_7m, p12\_7e and p59\_7k. Among the three molecules, p59\_7m exhibits the lowest binding free energy of -24.20 kcal/mol. p59\_7m forms the most extensive and stable hydrogen bond and hydrophobic interactions with M<sup>Pro</sup> active site residues THR 26, HIS 41, MET 49, ASN 142, CYS 145 and ARG 188, which are shown to interact with peptidomimetic inhibitors in the crystal structures [7,32]. Different from the peptidomimetic inhibitors in the crystal structures which spans S1' to S4 pocket, p59\_7m binds at S2' to S2 pocket. The carboline derivative p59\_7m is worthy of further investigation.

SARS-CoV-2 may predispose to both venous and arterial thromboembolic disease due to excessive inflammation, hypoxia, immobilization and diffuse intravascular coagulation [33]. Previous works indicate carboline and quinoline molecules decrease both arterial and venous thrombus *in vivo* [34,35]. Also, carboline and quinoline molecules may have anti-inflammatory activity [34,36]. Therefore, the selected carboline derivatives may also have the potential of reducing thrombus and inflammatory syndromes of SARS-CoV-2 in the future perspective.

## Conclusion

Among 2598 molecules in the database we established, the top 12 molecules were selected through the docking-based virtual screening using AutoDock Vina. Then MD simulations were performed on the apo form and the 12 docked complexes of SARS-CoV2 M<sup>Pro</sup> and molecules to confirm their system stabilities. Based on the MD simulations, binding affinities of the 12 molecules with SARS-CoV-2 M<sup>Pro</sup> were calculated using MM-PBSA method. The top three molecules p59\_7m, p12\_7e and p59\_7k bind SARS-CoV-2 M<sup>Pro</sup> with the lowest MM-PBSA binding free energies of -24.20, -17.98, -17.67 kcal/mol, respectively. They form extensive hydrogen bonds with the active site residues and obviously decreased the flexibility of SARS-CoV-2 M<sup>Pro</sup>. The selected three molecules are worthy of further bioactivity studies against SARS-CoV-2 M<sup>Pro</sup>. This result also encourages further exploration of bioactive carboline and quinoline derivatives against SARS-CoV-2.

## Future perspective

Previous works indicate carboline and quinoline molecules decrease both arterial and venous thrombus *in vivo*. Also, carboline and quinoline molecules have the anti-inflammatory activity *in vivo* from the previous research. Carboline, quinoline and their derivatives have the potential to be explored as antiviral molecules with anti-thrombosis and anti-inflammatory activities in the future.

### Summary points

- SARS-CoV-2 causes more than 3.8 million deaths according to the WHO.
- Drugs treating SARS-CoV-2 infection are in urgent need.
- The main protease (M<sup>Pro</sup>) of SARS-CoV-2 has become one of the most promising targets for new drugs.
- Carboline and quinoline molecules possess powerful antiviral bioactivities.
- An in-house database carboline and quinoline database containing 2598 carboline and quinoline molecules was established for the discovery of M<sup>Pro</sup> inhibitors.
- Docking-based virtual screening and following molecular dynamics simulations revealed three potential M<sup>Pro</sup> inhibitors p59\_7m, p12\_7e and p59\_7k.
- Among the three molecules, p59\_7m exhibits the lowest binding free energy of -24.20 kcal/mol.
- Similar to the peptidomimetic inhibitors in the crystal structures, p59\_7m forms extensive and stable hydrogen bonds and hydrophobic interactions with M<sup>Pro</sup> active site residues THR 26, HIS 41, MET 49, ASN 142, CYS 145 and ARG 188.
- The carboline derivative p59\_7m is worthy of further investigation of anti-SARS-CoV-2 activity.

### Author contributions

The authors contributed equally to this work.

### Acknowledgments

The authors thank Engineering Research Center of Endogenous Prophylactic of Ministry of Education of China for technical support.

### Financial & competing interests disclosure

This work was financially supported by Scientific Research Program of Beijing Municipal Education Commission (KM202110025024). The authors have no other relevant affiliations or financial involvement with any organization or entity with a financial interest in or financial conflict with the subject matter or materials discussed in the manuscript apart from those disclosed.

No writing assistance was utilized in the production of this manuscript.

### References

Papers of special note have been highlighted as: ● of interest

1. WHO Coronavirus Disease (COVID-19) Dashboard. World Health Organization, Geneva (2020). <https://covid19.who.int/>
2. Martínez MA. Compounds with therapeutic potential against novel respiratory 2019 coronavirus. *Antimicrob. Agents Chemother.* 64(5), e00399–20 (2020).
3. Yen J, Wang I, Yen T. COVID-19 vaccination & dialysis patients: why the variable response. *QJM-Mon. J. Assoc. Physicians* doi:10.1093/qjmed/hcab171 (2021) (Epub ahead of print).
4. Aschenbrenner DS. Remdesivir approved to treat COVID-19 amid controversy. *Am. J. Nurs.* 121(1), 22–24 (2021).
5. Luan B, Tien H, Cheng X, Lan G, Wang H. Targeting proteases for treating COVID-19. *J. Proteome Res.* 19(11), 4316–4326 (2020).
- **g\_Mmpbsa tools that performs more accurate calculation was used to calculate the free binding energy based on the data of molecular dynamics (MD).**
6. Boopathi S, Poma AB, Kolandaivel P. Novel 2019 coronavirus structure, mechanism of action, antiviral drug promises and rule out against its treatment. *J. Biomol. Struct. Dyn.* 39(9), 3409–3418 (2020).
7. Jin Z, Du X, Xu Y *et al.* Structure of M<sup>pro</sup> from COVID-19 virus and discovery of its inhibitors. *Nature* 582(7811), 289–293 (2020).
- **g\_Mmpbsa tools that performs more accurate calculation was used to calculate the free binding energy based on the data of MD.**
8. Al-Khafaji K, Al-Duhaidahawil D, Taskin Tok T. Using integrated computational approaches to identify safe and rapid treatment for SARS-CoV-2. *J. Biomol. Struct. Dyn.* 39(9), 3387–3395 (2021).
9. Ibrahim MaA, Abdelrahman AHM, Hegazy MEF. In-silico drug repurposing and molecular dynamics puzzled out potential SARS-CoV-2 main protease inhibitors. *J. Biomol. Struct. Dyn.* doi:10.1080/07391102.2020.1791958 (2020) (Epub ahead of print).
10. Ibrahim MaA, Mohamed EaR, Abdelrahman AHM *et al.* Rutin and flavone analogs as prospective SARS-CoV-2 main protease inhibitors: *in silico* drug discovery study. *J. Mol. Graph* 105, 107904 (2021).
11. Ibrahim MaA, Abdelrahman AHM, Mohamed TA *et al.* In silico mining of terpenes from red-sea invertebrates for SARS-CoV-2 main protease (M-pro) inhibitors. *Molecules* 26(7), 2082 (2021).
12. Ibrahim MaA, Abdelrahman AHM, Allemailem KS, Almatroudi A, Moustafa MF, Hegazy M-EF. In silico evaluation of prospective anti-COVID-19 drug candidates as potential SARS-CoV-2 main protease inhibitors. *Protein J.* 40(3), 296–309 (2021).
13. Ibrahim MaA, Abdeljawaad KaA, Abdelrahman AHM, Hegazy MEF. Natural-like products as potential SARS-CoV-2 M(pro)inhibitors: in-silicodrug discovery. *J. Biomol. Struct. Dyn.* doi:10.1080/07391102.2020.1790037 (2020) (Epub ahead of print).
14. Ibrahim MaA, Abdelrahman AHM, Hussien TA *et al.* In silico drug discovery of major metabolites from spices as SARS-CoV-2 main protease inhibitors. *Comput. Biol. Med.* 126, 0010–4825 (2020).
15. Wink M. Modes of action of herbal medicines and plant secondary metabolites. *Medicines (Basel)* 2(3), 251–286 (2015).
- **Some of plant secondary metabolites, carboline and quinoline derivatives show powerful antiviral bioactivity which encourage us to explore carboline and quinoline in our in-house database against SARS-CoV-2 virus.**
16. Kintzer AF, Stroud RM. Structure, inhibition and regulation of two-pore channel TPC1 from *Arabidopsis thaliana*. *Nature* 531(7593), 258 (2016).
- **Some of plant secondary metabolites, carboline and quinoline derivatives show powerful antiviral bioactivity which encourage us to explore carboline and quinoline in our in-house database against SARS-CoV-2 virus.**
17. O'Boyle NM, Banck M, James CA, Morley C, Vandermeersch T, Hutchison GR. Open Babel: an open chemical toolbox. *J. Cheminformatics* 3, 14 (2011).
18. Elmezayen AD, Al-Obaidi A, Sahin AT, Yeleki K. Drug repurposing for coronavirus (COVID-19): *in silico* screening of known drugs against coronavirus 3CL hydrolase and protease enzymes. *J. Biomol. Struct. Dyn.* 39(8), 2980–2992 (2020).

19. Kuca K, Musilek K, Jun D *et al.* A newly developed oxime K203 is the most effective reactivator of tabun-inhibited acetylcholinesterase. *BMC Pharmacol. Toxicol.* 19(1), 8 (2018).
20. De Lima WEA, Pereira AF, De Castro AA, Da Cunha EFF, Ramalho TC. Flexibility in the molecular design of acetylcholinesterase reactivators: probing representative conformations by chemometric techniques and docking/QM calculations. *Lett. Drug Des. Discov.* 13(5), 360–371 (2016).
21. Bianco G, Forli S, Goodsell DS, Olson AJ. Covalent docking using AutoDock: two-point attractor and flexible side chain methods. *Protein Sci.* 25(1), 295–301 (2016).
22. Al-Khafaji K, Tok TT. Understanding the mechanism of amygdalin's multifunctional anti-cancer action using computational approach. *J. Biomol. Struct. Dyn.* 39(5), 1600–1610 (2021).
23. Shukla R, Munjal NS, Singh TR. Identification of novel small molecules against GSK3 beta for Alzheimer's disease using chemoinformatics approach. *J. Mol. Graph.* 91, 91–104 (2019).
24. Vanommeslaeghe K, Hatcher E, Acharya C *et al.* CHARMM general force field: a force field for drug-like molecules compatible with the CHARMM all-atom additive biological force fields. *J. Comput. Chem.* 31(4), 671–690 (2010).
25. Abraham MJ, Murtola T, Schulz R *et al.* GROMACS: high performance molecular simulations through multi-level parallelism from laptops to supercomputers. *SoftwareX* 1–2, 19–25 (2015).
26. Huang J, Mackerell AD. CHARMM36 all-atom additive protein force field: validation based on comparison to NMR data. *J. Comput. Chem.* 34(25), 2135–2145 (2013).
27. Kusalik PG, Svishchev IM. The spatial structure in liquid water. *Science* 265(5176), 1219–1221 (1994).
28. Darden T, York D, Pedersen L. Particle mesh Ewald – an N.log(N) method for Ewald sums in large systems. *J. Chem. Phys.* 98(12), 10089–10092 (1993).
29. Kumari R, Kumar R, Lynn A. Open Source Drug Discovery C. g\_mmpbsa-A GROMACS tool for high-throughput MM-PBSA calculations. *J. Chem. Inf. Model.* 54(7), 1951–1962 (2014).
- **g-Mmpbsa tools that performs more accurate calculation was used to calculate the free binding energy based on the data of MD.**
30. Altis A, Nguyen PH, Hegger R, Stock G. Dihedral angle principal component analysis of molecular dynamics simulations. *J. Chem. Phys.* 126(24), 244111 (2007).
31. Vandyck K, Deval J. Considerations for the discovery and development of 3-chymotrypsin-like cysteine protease inhibitors targeting SARS-CoV-2 infection. *Curr. Opin. Virol.* 49, 36–40 (2021).
32. Zhang LL, Lin DZ, Sun XYY *et al.* Crystal structure of SARS-CoV-2 main protease provides a basis for design of improved alpha-ketoamide inhibitors. *Science* 368(6489), 409 (2020).
33. Klok FA, Kruip MJHA, Van Der Meer NJM *et al.* Incidence of thrombotic complications in critically ill ICU patients with COVID-19. *Thromb. Res.* 191, 145–147 (2020).
34. Zhu H, Wang Y, Song C *et al.* Docking of THPDTPi: to explore P-selectin as a common target of anti-tumor, anti-thrombotic and anti-inflammatory agent. *Oncotarget* 9(1), 268–281 (2018).
- **As a carboline derivative, THPDTPi shows anti-thrombosis and anti-inflammation activity in animal models.**
35. Zheng M, Zhang X, Zhao M *et al.* (3S)-N-(L-Aminoacyl)-1,2,3,4-tetrahydroisoquinolines, a class of novel antithrombotic agents: synthesis, bioassay, 3D QSAR, and ADME analysis. *Bioorg. Med. Chem.* 16(21), 9574–9587 (2008).
- **As quinoline derivatives, (3S)-N-(L-aminoacyl)-1,2,3,4-tetrahydroisoquinolines show anti-arterial thrombosis activity in a rat model.**
36. Wu J, Zhu H, Yang G *et al.* Design and synthesis of nanoscaled IQCA-TAVV as a delivery system capable of antiplatelet activation, targeting arterial thrombus and releasing IQCA. *Int. J. Nanomed.* 13, 1139–1158 (2018).
- **As a quinoline derivative, IQCA-TAVV shows anti-arterial thrombosis activity in both rat and mouse models.**